Volume 1 | Number 1 | Jan 2013 | Pages 1–100

PCCP

Physical Chemistry Chemical Physics
www.rsc.org/pccp

ROYAL SOCIETY OF CHEMISTRY

ROYAL SOCIETY OF CHEMISTRY

www.rsc.org/pccp

Visible-light photocatalysis in Cu$_2$Se nanowires with exposed {111} facets and charge separation between (111) and ($\bar{1}\bar{1}\bar{1}$) polar surfaces

Bin Liu[1], Lichao Ning[2], Hua Zhao[1], Congjie Zhang[2], Heqing Yang[1,*] and Shengzhong (Frank) Liu[3]

5   *1. Key Laboratory of Macromolecular Science of Shaanxi Province, School of Materials Science and Engineering, Shaanxi Normal University, Xi'an, 710119, China. Email: hqyang@snnu.edu.cn. 2. Key Laboratory of Macromolecular Science of Shaanxi Province, School of Chemistry and Chemical Engineering, Shaanxi Normal University, Xi'an, 710119, China. 3. Key Laboratory of Applied Surface and Colloid Chemistry, National Ministry of Education, School of Materials Science and Engineering, Shaanxi Normal University,*

10 *Xi'an 710119, China*

Abstract

The search for active narrow band gap semiconductor photocatalysts that directly split water or degrade organic pollutants under solar irradiation remains to be an open issue. We synthesized Cu$_2$Se nanowires with exposed {111} facets using ethanol and glycerol as morphology controlling agents.

15 The {111} facets were found to be the active facets for decomposing organic contaminants in entire solar spectrum. Based on the polar structure of the Cu$_2$Se {111} facets, a charge separation model between polar (111) and ($\bar{1}\bar{1}\bar{1}$) surfaces is proposed. The internal electric field between polar (111) and ($\bar{1}\bar{1}\bar{1}$) surfaces created by the spontaneous polarization drives charge separation. The reduction and oxidation reactions take place on the positive (111) and negative ($\bar{1}\bar{1}\bar{1}$) polar surfaces, respectively.

20 This suggests the surface-engineering of narrow band gap semiconductors as a strategy to fabricate photocatalysts with high reactivity in entire solar spectrum. The charge separation model can deepen understanding of charge transfer in the other semiconductor nanocrystals with highly photocatalytic activities and offer guidance to design more effective photocatalysts as well as new type of solar cells, photoelectrodes and photoelectric devices.

1 Introdution

Photocatalysis has received much attention as a potential solution to the worldwide energy shortage[1, 2] and for counteracting environmental degradation.[1,3] The key issue in photocatalysis is to develop photocatalysts with high catalytic activities. Since the discovery of photoinduced decomposition of water on TiO_2 electrodes,[4] the photocatalytic activities of TiO_2,[5, 6] ZnO,[7] $BiOCl$,[8] $InOOH$,[9] WO_3,[10] Ag_3PO_4,[11] CdS,[12] ZnS[13] $ZnSe$,[14] $ZnS–CuInS_2–AgInS_2$,[15] $NiO_x/In_{1-x}Ni_xTaO_4$,[16] $TiO_{2-x}C_x$,[17] $Ga_{1-x}Zn_x(N_{1-x}O_x)$,[18] $Sm_2Ti_2O_5S_2$,[19] $TiO_{2-x}N_x$,[20] CdS loaded with MoS_2,[21] $Pt-RuO_2/Zn_2GeO_4$[22] and Ag_3PO_4.[23] in the degradation of toxic organic pollutants, splitting of water and reduction of CO_2 have been extensively studied. However, the search for more effective semiconductor photocatalysts remains to be an open issue. Regarding optical absorption, narrow bandgap semiconductors are more likely to exhibit high absorbance and hence more efficient for harvesting low energy photons. However, the recombination probability for photoexcited electron-hole pairs is rather high in these types of semiconductors, and thus the narrow band gap semiconductor photocatalysts show generally poor catalytic performance[1].

Cu_2Se, an important p-type semiconductor with a widely varying indirect band gap of 1.1–1.5 eV and a direct band gap between 2.0–2.3 eV,[24] has been considered as a potential candidate for many green energy devices, such as solar cells, lithium batteries, supercapacitors, and thermoelectric devices.[25–27] However, there has been no report in literature so far on study of photocatalytic behavior of Cu_2Se semiconductor.

The crystal facet engineering of semiconductors has been proven to be an effective strategy to increase photocatalytic performances.[1,5–12] Herein, we first report on the controllable synthesis of Cu_2Se nanowires with exposed {111} facets and various aspect ratios and the aspect ratio-dependent photoreactivity for degradation of malachite green (MG) under visible light. The superior

photocatalytic activity is attributed to the exposed {111} facets. Structure and atomic charge distribution of the cubic phase Cu_2Se {111} facets were studied by periodic density functional theory (DFT) calculations. Based on the polar structure of the {111} facets, a charge separation model between polar (111) and ($\bar{1}\,\bar{1}\,\bar{1}$) surfaces is proposed to explain the enhanced photocatalytic activities.

2 Experimental

Catalyst preparation

The Cu_2Se nanowires with various aspect ratios were prepared as follows: In a typical procedure, 0.100 g $Cu(Ac)_2 \cdot H_2O$ (0.5 mmol), 0.039 g of Se powder (0.5 mmol), 1.200 g NaOH, 15.0 or 20.0 mL of ethanol and 10.0 or 5.0 mL of glycerol ($C_3H_8O_3$) were added in order into a Teflon-lined autoclave of 50 mL capacity, After the mixture was stirred for 30 min, the autoclave was sealed and heated at 200 ^{o}C for 6 or 12 h. After the heating treatment, the autoclave was cooled to room temperature naturally. The products were collected by centrifugation, washed three times with de-ionized water and absolute ethanol, respectively. Finally, the product was dried under vacuum and stored in a vacuum desiccators.

Characterizations

The as-prepared products were characterized and analyzed using powder X-ray diffraction (XRD), scanning electron microscopy (SEM), transmission electron microscopy (TEM), Infrared (IR) spectroscopy and X-ray photoelectron spectra (XPS). The XRD patterns were obtained by using a DX-2700 X-Ray diffractometer equipped with Cu Kα_1 radiation (λ = 1.541 Å) at 40 kV and 30 mA. Each specimen was at a step size of 0.02^o and a scanning speed of 8° /min scanned with diffraction angles varying between 20 and 70°. The SEM images were obtained using a FEI Quanta 200 scanning electron microscope at an accelerating voltage of 25 kV. The TEM and electron diffraction images were obtained using a JEOL JEM-2100 transmission electron microscope at an accelerating voltage of 200 kV. The IR spectrum was recorded using a Brucher EQUINX55 Fourier transform IR spectrophotometer at room temperature. The XPS measurements were performed by using a Kratos

75　Axisultra X-ray photoelectron spectrometer with an excitation source of $Al_{K\alpha} = 1486.7$ eV. Brunauer-Emmett-Teller (BET) specific surface area measurement was performed by N_2 gas adsorption using an America Micromeritics ASAP 2020 surface analytical instrument. Diffuse reflectance spectrum of the products was obtained on a Perkin Elmer Lambd 950 spectrophotometer.

Periodic DFT calculations

80　Crystal structure of Cu_2Se was calculated by using the DMOL3 code,[28] and this structure is an idealized model of the high temperature β-phase of Cu_2Se.[29] The atomic charges are computed using Hirshfeld[30] population analyses. The DFT calculations for the surface energy were carried out with the CASTEP plane wave code[31] using the generalized gradient approximation (GGA) with Perdew-Burke-Ernzerhof (PBE) exchange-correlation functional.[32] Ultrasoft pseudopentionals were

85　expanded by a plane-wave basis set with a cutoff energy of 320 eV employed throughout the model. The self-consistent field convergence on total energy was set to 1×10^{-5} eV. The structural optimization for the bulk and slabs were considered completely when energies were converged to better than 1×10^{-5} eV per atom, atomic displacements, maximum forces and maximum stresses were converged to 1×10^{-3} Å, 3×10^{-2} eV/Å, and 5×10^{-2} GPa, respectively. A k-point separation ($2\pi \times 0.015$ Å) was used to

90　generate the k-point grid. The (111) surface was modeled by a 24-layer slab and the $(1\bar{2}1)$ and $(\bar{2}02)$ surfaces were modeled by a 16-layer slab, which are sufficient to converge the surface energy to within 0.02 J/m^2. Geometry relaxations were performed with the midlayers fixed, the vacuum separation between the slabs was 15 Å, and all the surfaces considered in this work were stoichiometric. The surface energies were computed using the formula[33]:

95
$$E_{surface} = \frac{E_{slab} - nE_{bulk}}{2A}$$

where E_{slab} is the total energy of the slab, E_{bulk} is the total energy of the bulk per unit cell, n is the number of bulk unit cells contained in the slab, and A is the surface area of each side of the slab, the

1/2 factor is used to obtain the average value of the surface energies of the top and bottom of the slab. The E_{bulk} is obtained from the fomula[34]:

$$E_{bulk} = E_{salb}(n) - E_{salb}(n-1)$$

100

where n is the number of repeat units.

Photocatalytic activity test

MG with a molecular weight of 927, selected as a model organic compound to examine the photocatalytic activity of the Cu_2Se nanowires. 20.0 mg of the as-prepared Cu_2Se catalysts was added

105 to 20.0 mL of 2.5×10^{-5} M MG solution to get a suspension. The suspension was magnetically stirred for 10 min in the dark to establish an adsorption/desorption equilibrium between the dye and the catalyst. Then the mixed solution was irradiated by a Xe lamp (500 W) which is equipped with an optical filter ($\lambda \geq 420$ nm) to cut off the light in the ultraviolet region (XPA-7 photochemical reactor, Xujiang Electromechanical Plant, Nanjing, China). At a given irradiation time interval, 5 mL of

110 sample was withdrawn from the test tube for analysis. Sample solutions were obtained by centrifugation, and their absorption spectra were measured on a U-2910 ultraviolet–visible spectrophotometer (Hitachi High-Technologies Corporation, Tokyo, Japan) using de-ionized water as reference.

3 Results and discussion

115 The cubic phase Cu_2Se nanowires having {111} facets were synthesized by a solvothermal reaction of $Cu(Ac)_2$ with Se, NaOH, C_2H_5OH and $C_3H_8O_3$. Aspect ratio (length-to-diameter ratio) of the Cu_2Se nanowires can be changed by adjusting the reaction time and volume ratio of ethanol to glycerol. Representative SEM images of the as-synthesized Cu_2Se nanowires with various aspect ratios are shown in Fig. 1a–d. The corresponding synthesis parameters, diameters, lengths and aspect ratios of

120 the as-obtained Cu_2Se nanowires are summarized in Table 1. Aspect ratios of the samples 1, 2 and 3 are 13–20, 21–82 and 220–600, respectively. The upper-right inset of Fig. 1d shows a broken nanowire with rectangle-like cross section with a width-to-thickness ratio of 1.4.

5

Table 1

Diameters, lengths, aspect ratios, percentages of {111}, TC (111), k and k' of the Cu_2Se nanowires obtained via changing the solvothermal reaction time and the volume ratios of ethanol and glycerol.

Sample no	Ethanol (mL)	Glycerol (mL)	Time (h)	Diameter (μm)	Length (μm)	Aspect ratio	The percentage of {111}	TC(111)	k (min^{-1})	k' [a] (min^{-1}m^{-2})
1	20	5	12	1.42-3.57	19-29	13-20	55.2~56.7%	1.5	0.0721 ±0.0014	0.096
2	15	10	6	0.65-2.14	45-53	21-82	60.1~61.0%	1.8	0.1346 ±0.0024	0.157
3	15	10	12	0.14-0.30	66-84	220-600	70.2~72.1%	2.1	0.2324 ±0.0010	0.200

[a] k': Normalized apparent rate constant of the degradation per unit surface.

Fig. 2 exhibits corresponding XRD patterns of the Cu_2Se nanowires with various aspect ratios. All the diffraction peaks of the XRD patterns could be perfectly indexed to pure cubic Cu_2Se (Joint Committee on Powder Diffraction Standards (JCPDS) card no. 65−2982), suggesting that all the as-synthesized nanowires are cubic structured Cu_2Se crystals. Moreover, it is found that the present nanowires show markedly higher intensity ratios of (111) to other diffraction peaks in comparison with those from standard pattern of the cubic Cu_2Se powder samples, demonstrating strong (111) preferred orientation. The (111) peak intensity increases with an increase on the aspect ratio, indicating (111) orientation is enhanced. The texture coefficient of (111) plane (TC (111)) is defined as[9] :

$$TC(111) = \frac{I(111)}{I_0(111)} \left\{ \frac{1}{n} \sum \frac{I(hkl)}{I_0(hkl)} \right\}^{-1}$$

Where I (h k l) are measured intensities of (h k l) reflection, I_0 (h k l) are powder diffraction intensities of cubic Cu_2Se according to the JCPDS card no. 65−2982, and n is the number of diffraction peaks used in the calculation. For materials with random crystallographic orientations, e.g. powders, the texture coefficient of any (h k l) reflection should be 1. The TC (111) values for samples 1, 2 and 3 were measured to be 1.5, 1.8 and 2.1, respectively (see Table 1).

Fig. 3a presents a representative TEM image of a Cu_2Se nanowire with a diameter of about 90 nm from sample 3. Fig. 3b and c show selected area electron diffraction (SAED) pattern and high-

resolution TEM (HRTEM) image from the box in (a), respectively. The SAED pattern can be indexed

to [111] zone axis of single-crystalline Cu_2Se with the cubic structure. The lattice spacing of 0.20 nm

between adjacent lattice planes corresponds to the distance between two { $\bar{2}02$ } facets. The SAED and

HRTEM results indicate that the Cu_2Se nanowires grow along [$\bar{2}02$] direction, are mainly enclosed by

(111), $(\bar{1}\bar{1}\bar{1})$, $(1\bar{2}1)$ and $(\bar{1}2\bar{1})$ facets. The schematic illustration of crystal orientation of the Cu_2Se

nanowires is shown in Fig. 3d. Percentages of {111} surfaces for samples 1, 2 and 3 were calculated,

the results are shown in Table 1. It can be seen that the percentage of {111} surfaces increase with an

increase on the aspect ratios.

The diffuse reflectance spectrum of sample 3 is shown in Fig. 4, which reveals that Cu_2Se

nanowires absorb appreciably at wavelengths ≤ 1400 nm. As a crystalline semiconductor, the optical

absorption near the band edge follows the formula[35]:

$$\alpha h v = A(h v - E_g)^{n/2}$$

Where α, v, E_g and A are the absorption coefficient, light frequency, band gap energy, and a constant,

respectively. Among them, n depends on the characteristics of the transition in a semiconductor, i.e.,

direct transition (n=1) or indirect transition (n=4). For Cu_2Se, the value of n is 4 for indirect transition.

The band gap energy (Eg value) of Cu_2Se can be thus estimated from a plot of $(\alpha h v)^{1/2}$ versus photon

energy ($h v$) (inset in Fig. 4), and the result is found to be about 0.87 eV.

In order to identify the role of NaOH in the formation of Cu_2Se nanowires, the products obtained

by a reaction of $Cu(Ac)_2$ with Se in the mixed solvent of 15 mL of ethanol and 10 mL of glycerol at

200 ^oC for 12 h were characterized using SEM and XRD, and the results are shown in Fig. 5a and b. It

is found that the as-obtained products without NaOH are composed of flake-like structures with the

widths of 1.2–2.5 um and thicknesses of 400–800 nm instead of wire-like structures. The

corresponding XRD pattern (Fig. 5b) demonstrates that the as-prepared flake-like products are mixture

of CuSe with a hexagonal structure and Se with a rhombohedral structure instead of cubic Cu_2Se.

Therefore, the NaOH plays an important role in the formation Cu_2Se. The C_2H_5OH or $C_3H_8O_3$ works

as a reducing agent in the solvothermal reaction system. In the presence of NaOH, elemental Se and Cu^{2+} ions are reduced by C_2H_5OH or $C_3H_8O_3$ into Se^{2-} and Cu^+ ions, respectively.[36–38] The Cu^+ ions react with Se^{2-} ions to form Cu_2Se. The chemical reactions to form Cu_2Se are formulated as follows:

$$Se + C_2H_5OH \text{ or } C_3H_8O_3 \xrightarrow{\text{NaOH}} Se^{2-} \qquad (1)$$

$$Cu^{2+} + C_2H_5OH \text{ or } C_3H_8O_3 \xrightarrow{\text{NaOH}} Cu^+ \qquad (2)$$

$$Cu^+ + Se^{2-} \longrightarrow Cu_2Se \qquad (3)$$
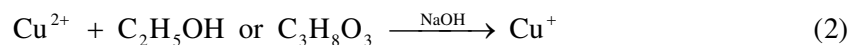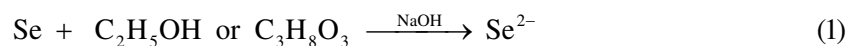
The products obtained in 25 mL of ethanol and a mixed solvent of 10 mL of ethanol and 15 mL of glycerol by the solvothermal method were characterized by SEM and XRD. The results indicate that the products obtained in pure ethanol are composed of cubic phase Cu_2Se wire-like structures with the diameters of 0.42–1.66 μm and lengths of 6.25–15.5 μm and Cu_2Se particles with irregular morphology (Fig. 6a and b). The products obtained in the mixed solvent of 10 mL of ethanol and 15 mL glycerol consist of cubic structured Cu_2Se flake-like structures with the diameters of 2.25–7.51 μm and thicknesses of 0.41–0.83 μm and Cu_2Se particles with irregular morphology (Fig. 6c and d). These results reveal that the Cu_2Se nanowires can be obtained in the mixed solvent with $V_{ethanol}/V_{glycerol}$ of 4:1~3:2.The glycerol and ethanol play a vital role in the formation of the Cu_2Se wire-like structures.

The IR spectrum of sample 3 was measured, and the result is shown in Fig. 7. In the IR spectrum, the two bands at 3466 and 1632 cm^{-1} are assigned to the O–H stretching and bending vibrations, respectively.[9,39] The bands at 2926 and 2854 cm^{-1} are attributed to the asymmetrical and symmetrical stretching vibrations of $-CH_2$, respectively.[9,40] Two bands at 1382 and 1353 cm^{-1} may correspond to C–H bending vibration of CH, CH_2 and CH_3 groups.[9, 40] The IR spectrum suggests that there are ethanol and glycerol molecules on the surface of the Cu_2Se nanowires.

To further confirm the chemical composition and valence state, an XPS analysis was performed. The binding energies obtained in the XPS analysis were corrected for specimen charging through referencing the C1s to 284.6 eV. The XPS spectra of sample 3 are shown in Fig. 8, including (a) the

survey spectrum, (b) Cu $2p_{3/2}$ and $2p_{1/2}$, (c) Se $3d_{5/2}$ and $3d_{3/2}$, (d) C 1s and (e) O 1s. The $Cu2p_{3/2}$ and $Cu2p_{1/2}$ peaks were symmetric, narrow, and devoid of satellite peak. The observed value of the binding energy for Cu $2p_{3/2}$ and $Cu_{1/2}$ was 931.5 and 951.4 eV, respectively, which is in agreement with the values reported for Cu_2Se nanoparticles[24,25] and dendritic architectures.[26] The binding energy for Se

195 $d3_{5/2}$ and $3d_{3/2}$ was 54.1 and 54.8 eV, respectively, which is close to the values reported for Se.[24,25] The C 1s XPS is dominated by a large peak at 282.6 eV and a second feature at about 285.5 eV binding energies, which is attributed to C 1s of C-C and C-O,[41,42] respectively. The O 1s XPS is dominated by a large peak at 529.7 eV and a second feature at about 532.3 eV binding energies, which corresponds to O 1s of O-Cu and O-H,[41,42] respectively. The XPS data further indicates that ethanol and glycerol

200 may be adsorbed on the surface of the Cu_2Se nanowires.

The cubic Cu_2Se crystal structure is shown in Fig. 9a. The Cu atom is tetrahedrally coordinated to four Se atoms. The Se atoms are coordinated to eight Cu atoms in a cube. The atomic structures of (111) and $(1\bar{2}1)$ surfaces obtained from periodic DFT calculations are shown in Fig. 9b and c, respectively. Obviously, the (111) surface termination consists of two layers of unsaturated Cu sites,

205 and Cu atoms on the (111) plane are one or three coordinated Cu. The $(1\bar{2}1)$ surface termination consists of a layer of unsaturated Cu and Se sites, and the coordination number of Cu atoms on the $(1\bar{2}1)$ plane are two or three. In the solvothermal system, glycerol and ethanol may serve as ligands to Cu, and adsorbs selectively on the (111) and $(1\bar{2}1)$ prismatic faces of the Cu_2Se nanowires. The most likely structures are described in Fig. 9d and e, respectively. The presence of glycerol and ethanol

210 impedes the (111) and $(1\bar{2}1)$ plane growth, and thus Cu_2Se nanowires grow along the $[\bar{2}02]$ direction, leading to form Cu_2Se nanowires having {111} and $(1\bar{2}1)$ facets.

To demonstrate the potential applicability in photocatalysis of the as-obtained Cu_2Se nanowires, we investigated photocatalytic activity of the Cu_2Se nanowires using degradation of MG as a reference. Before evaluation of the photocatalytic activity, adsorption capacity of the as-prepared Cu_2Se samples

215 for MG was studied, and the results are shown in Fig. 10a. Fig. 10a shows the kinetics of MG

adsorption on the Cu_2Se powders (Fig. S1, Supporting Information) and samples 1, 2 and 3. The C_0 and C represent the concentration of MG at initial and any time, respectively. For Cu_2Se powders and samples 1, 2 and 3, after 10 min, the value of C/C_0 was 0.942, 0.938, 0.935 and 0.940, respectively and hardly decreased with an increase on the time, indicating an adsorption/desorption equilibrium between the dye and the Cu_2Se photocatalysts is achieved within 10 min. Therefore, the suspension containing the dye and the catalysts was stirred for 10 min in the dark before the Xe lamp irradiation to establish an adsorption/desorption equilibrium between the dye and the photocatalyst.

Fig. 10b shows the decomposition of MG in solution over Cu_2Se powders and samples 1, 2 and 3. The decomposition of the MG barely progresses without catalyst (curve I) under visible light irradiation ($\lambda \geq 420$ nm). When Cu_2Se powders and Cu_2Se nanowires are introduced into the system, the MG concentration decreases quickly over time (curve II–V). The decomposition rate over the Cu_2Se nanowires is higher than that over Cu_2Se powders, and it increases with the aspect ratios of Cu_2Se nanowires (curve III-V).

The fittings of ln (C_0/C) plot vs. time over Cu_2Se powders and samples 1, 2 and 3 are shown in Fig. 10c. The photodegradation of MG catalyzed by the four kinds of catalysts can be explained using pseudo first-order reaction. i.e. ln $(C_0/C) = kt$, where k is the apparent rate constant of the degradation. In our experiment, the k value is found to be 0.0133 ± 0.0007, 0.0721 ± 0.0014, 0.1346 ± 0.0024 and 0.2324 ± 0.0010 min^{-1}. It is generally accepted that the catalytic process is mainly related to the adsorption and desorption of molecules on the catalyst surface. The BET surface area of Cu_2Se powders and samples 1, 2 and 3 was measured to be 22.1, 37.4, 42.7 and 58.2 m^2 g^{-1}, respectively. The apparent rate constant of the degradation per unit surface area of the four kinds of catalysts, as for the basis for the comparison, is examined in this work. It is found that the normalized k' value for sample 3 is much larger than that for samples 1, 2 and Cu_2Se powders, as seen in Fig. 10d and Table 1, indicating that the photocatalytic activity of the as-prepared Cu_2Se nanowires is enhanced by increasing the aspect ratio, percentage of {111} surfaces and TC (111). It is reasonable to conclude that the exposed {111} facets may be highly reactive facets for degradation of MG.

10

The surface energy of the (111), $(1\bar{2}1)$ and $(\bar{2}02)$ facets of Cu_2Se nanowires was calculated using DFT, and the results are shown in Fig. S2 and Table S1, Supporting Information. It is found that Cu_2Se (111) facet has much higher surface energy, 1.00, comparing to 0.39 for $(1\bar{2}1)$ and 0.26 J/m^2 for $(\bar{2}02$) facets, indicating that the exposed (111) facet should be more reactive than $(1\bar{2}1)$ and $(\bar{2}02)$ facets[10,11]. As shown in Fig. 9b and c, the exposed $(1\bar{2}1)$ facet is non-polar surface, which is terminated with Cu and Se atoms. However, the exposed {111} facets are polar surfaces, they consist of a positive polar (111) plane terminated with Cu atoms, and a negative polar $(\bar{1}\bar{1}\bar{1})$ plane terminated with Se atoms. The atomic charges distribution of {111} facets from periodic DFT calculations is shown in Fig. 11a. Each layer contains all positive Cu^+ ions or all negative Se^{2-} ions in the [111] direction, the polar chain is shown in Fig. 11b. Cu atomic charge on the Cu-Cu_2Se (111) surface is +0.043 and Se atomic charge on the Se-Cu_2Se $(\bar{1}\bar{1}\bar{1})$ is −0.175. An internal electric field thus is established between the positive Cu-Cu_2Se (111) and negative Se-Cu_2Se $(\bar{1}\bar{1}\bar{1})$ polar surfaces due to the spontaneous polarization. A charge separation model between polar (111) and $(\bar{1}\bar{1}\bar{1})$ surfaces is thus proposed to explain the enhanced photocatalytic activities.

When the Cu_2Se nanowires with exposed {111} facets were employ as a photocatalyst, photogenerated electrons and holes migrate to the positive Cu-Cu_2Se (111) and negative Se-Cu_2Se $(\bar{1}\bar{1}\bar{1})$ polar surfaces, respectively, under the internal electric field (Fig. 11c). The reduction and oxidation reactions selectively take place on the positive Cu-Cu_2Se (111) and negative Se-Cu_2Se $(\bar{1}\bar{1}\bar{1})$ polar surfaces. The good charge separation can effectively reduce the probability of recombination of photogenerated electrons and holes, and thus the Cu_2Se nanowires with exposed {111} facets show superior photocatalytic activity comparing to the Cu_2Se powders. The photocatalytic activity of the Cu_2Se nanowires is further enhanced by increasing percentage of {111} surfaces, the aspect ratio and TC (111).

Moreover, we carried out the MG bleaching experiment repeatedly four times by using the sample 3 as a catalyst. As shown in Fig. 12, their photocatalytic activity was lightly lowered after four cycles,

11

which indicated that the as-prepared Cu$_2$Se nanowires exhibit remarkable photocatalytic stability. In addition, SEM images and XRD patterns of the sample 3 after four cycles was measured, and the results are shown in Fig. S3, Supporting Information. The SEM and XRD observations reveal that after the photocatalytic degradation experiment the products still consist of Cu$_2$Se nanowires. However, after the photocatalytic test intensity of the Cu$_2$Se diffraction peaks decreased, indicating its crystalline became poor. The fall in Cu$_2$Se crystalline may result in the decrease in the photocatalytic activity.

4 Conclusions

In summary, Cu$_2$Se nanowire with exposed {111} facets and various aspect ratios have been synthesized by adjusting synthesis parameters. The role of ethanol and glycerol in the formation of the Cu$_2$Se nanowires was investigated, and a possible mechanism was proposed. The cubic phase Cu$_2$Se {111} polar surfaces were found to be highly reactive facets for degradation of MG. Based on the polar structure of the {111} surfaces, a charge separation model between polar (111) and ($\bar{1}\,\bar{1}\,\bar{1}$) surfaces was proposed. The charge separation model may be applied to other semiconductor nanocrystals with highly photocatalytic activities. Our results demonstrate that it is feasible to obtain visible-light photocatalysts with excellent performance by the surface-engineering of narrow band gap semiconductor. The present study inspired us to design more effective photocatalysts and new type of photoelectrodes, solar cells and photoelectric devices.

Supporting Information

Preparation, SEM image and XRD pattern of Cu$_2$Se powders, Relaxed geometries and surface energies for the (111), (1$\bar{2}$1) and ($\bar{2}$02) surfaces of Cu$_2$Se, SEM image and XRD pattern of the sample 3 after four cycles.

Ackonwledgements

References

1 H. Tong, S. X. Ouyang, Y. P. Bi, N. Umezawa, M. Oshikiri, M. Oshikiri, J. H. Ye, *Adv. Mater.*, 2012, **24**, 229−251.

2 J. H. Yang, D. G. Wang, H. X. Han, C. Li, *Acc. Chem. Res.*, 2013, **46**, 1900−1909.

3 M.R. Hoffmann, S.T. Martin, W.Y. Choi, D.W. Bahnemann, *Chem. Rev.*, 1995, **95**, 69−96.

4 A. Fujishima, K. Honda, *Nature*, 1972, **238**, 37−38.

5 H. G. Yang, G. Liu, S. Z. Qiao, C. H. Sun, Y. G. Jin, S. C. Smith, J. Zou, H. M. Cheng, G. Q. Lu, *J. Am. Chem. Soc.*, 2009, **131,** 4078−4083.

6. M. Zhao, H. Xu, H. R. Chen, S. X. Ouyang, N. Umezawa, D. F. Wang, J. H. Ye, *J. Mater. Chem. A.*, 2015, **DOI:** 10.1039/C4TA06087C.

7 E. S. Jang, J. H. Won, S. J. Hwang, J. H. Choy, *Adv. Mater.*, 2006, **18**, 3309−3312.

8 J. Jiang, K. Zhao, X. Y. Xiao, L. Z. Zhang, *J. Am. Chem. Soc.*, 2012, **134**, 4473−4476.

9 H. Zhao, W. Y. Yin, M. Y. Zhao, Y. Z. Song, H. Q. Yang, *Appl. Catal., B*: *Environ.*, 2013, **130**, 178−186.

10 D. Q. Zhang, S. L. Wang, J. Zhu, H. X. Li, Y. F. Lu, *Appl. Catal., B*: *Environ.*, 2012, **123**, 398−404.

11 Y. P. Bi, S. X. Ouyang, N. Umezawa, J. Y. Cao, J. H. Ye, *J. Am. Chem. Soc.*, 2011, **133**, 6490−6492.

12 R. Jin, M.Y. Su, J. Wang, P. Zhang, M. Cui, Y. Chen, H. Q. Yang, *Mater. Res. Bull.*, 2012, **47**, 3070−3077.

13 X. Y. Wang, L. H. Zhang, H. Yang, S. Tian, X.W. Wang, L.N. Zhang, B. Liu, J. *Nanosci. Nanotechnol.*, 2010, **10**, 8387−8394.

14 L. H. Zhang, H. Q. Yang, J. Yu, F. H. Shao, L. Li, F. H. Zhang, H. Zhao, *J. Phys. Chem. C*, 2009, **113**, 5434−5443.

15 I. Tsuji, H. Kato, A. Kudo, Angew. *Chem. Int. Ed.*, 2005, **44**, 3565−3568.

16 Z. G. Zou, J. H. Ye, K. Sayama, H. Arakawa, *Nature*, 2001, **414**, 625−627.

17 S. U. M. Khan, M. Al-1Shahry, W. B. Ingler Jr, *Science*, 2002, **297**, 2243−2245.

18 D. L. Lu, T. Takata, N. Saito, Y. Inoue, K. Domen, *Nature*, 2006, **440**, 295.

19 A. Ishikawa, T. Takata, J. N. Kondo, M. Hara, H. Kobayashi, K. Domen, *J. Am. Chem. Soc*., 2002, **124**, 13547−13553.

20 R. Asahi, T. Morikawa, T. Ohwaki, K. Aoki, Y. Taga, *Science*, 2001, **293**, 269−271.

21 X. Zong, H. J. Yan, G. P. Wu, G. J. Ma, F. Y. Wen, L. Wang, C. Li, *J. Am. Chem. Soc*., 2008, **130**, 7176−7177.

22 Q. Liu, Y. Zhou, J. H. Kou, X. Y. Chen, Z. P. Tian, J. Gao, S. C. Yan, Z. G. Zou, *J. Am. Chem. Soc*., 2010, **132**, 14385−14387.

23 Z. G. Yi, J. H. Ye, N. Kikugawa, T. Kako, S.X. Ouyang, H. Stuart-Williams, H. Yang, J. Y. Cao, W. J. Luo, Z. S. Li, Y. Liu, R. L. Withers, *Nat. Mater.*, 2010, **9**, 559−564.

24 S. C. Riha, D. C. Johnson, A. L. Prieto, *J. Am. Chem. Soc*., 2011, **133**, 1383−1390.

25 S. L. Liu, Z. S. Zhang, J. C. Bao, Y. Q. Lan, W. W. Tu, M. Han, Z. H. Dai, *J. Phys. Chem. C*, 2013, **117**, 15164−15173.

26 J. B. Zhu, Q. Y. Li, L. F. Bai, Y. F. Sun, M. Zhou, Y. Xie, *Chem. Eur. J.*, 2012, **18**, 13213−13221.

27 S. Deka, A. Genovese, Y. Zhang, K. Miszta, G. Bertoni, R. Krahne, C. Giannini, L. Manna, *J. Am. Chem. Soc.*, 2010, **132**, 8912−8914.

28 B. Delley, *J. Chem. Phys*., 1990, **92**, 508–517.

29 M. Rasander, L. Bergqvist, A. Delin, *J. Phys. Condens. Mat.*, 2013, **25**, 1–7.

30 F. L. Hirshfeld, *Theor. Chim. Acta.*, 1977, **44**, 129–138.

31 M. Segall, P. J. Lindan, M. a. Probert, C. Pickard, P. Hasnip, S. Clark, M. Payne, *J. Phys. Condens. Mat.*, 2002, **14**, 2717–2744.

14

32   J. P. Perdew, K. Burke, M. Ernzerhof, *Phys. Rev. Let*., 1996, **77**, 3865–3868.

340   33   J. C. Boettger, *Phys. Rev. B*., 1994, **49**, 16798–16800.

34.   C. Ruberto, Y. Yourdshahyan, B. I.Lundqvist, *Phys. Rev. B*., 2003, **67**, 195412.

35   Q. Liang, H. Zhao, L. C, Ning, J. L. Wang, C. J. Zhang, L. Wang, A. H. Wei, Q. Zhao, H. Q.

Yang, S. Z. Liu, *Appl. Catal., B*: *Environ*., 2013, **152**, 390–396.

36   L. H. Zhang, H. Q. Yang, X. L. Xie, F. H. Zhang, L. Li, *J. Alloys Compd*., 2009, **473**, 65–70.

345   37   B. Li, Y. Xie, J. X. Huang, Y. T. Qian, *Adv. Mater*., 1999, **11**, 1456–1459.

38   T. Jiang, G. A. Ozin, R. L. Bedard, *Adv. Mater*., 1994, **6**, 860–865.

39   A. H. Wei, B. Liu, H. Zhao, Y. Chen, W. L. Wang, Y. Ma, H. Q. Yang, S. Z. Liu, *Chem. Eng. J*.,

2014, **239**, 141–148.

40   B. Herreros, T. L. Barr, J. Klinowski, *J. Phys. Chem*., 1994, **98**, 738–741.

350   41   N. Gleason, J. Guevremont, F. Zaera, *J. Phys. Chem*., 2003, **107**, 11133–11141.

42   K. C. Popat, G. Mor, C. A. Grimes, T. A. Desar, *Langmuir*., 2004, **20**, 8035–8041.

355